*AAPS PharmSciTech, Vol. 15, No. 4, August 2014 (© 2014)*
DOI: 10.1208/s12249-014-0126-7

*Research Article*

*Theme: Advances in Formulation and Device Technologies for Pulmonary Drug Delivery*
*Guest Editors: Paul B. Myrdal and Steve W. Stein*

# *In Vitro* and *In Vivo* Performance of Dry Powder Inhalation Formulations: Comparison of Particles Prepared by Thin Film Freezing and Micronization

**Yi-Bo Wang,[1] Alan B. Watts,[1] Jay I. Peters,[2] Sha Liu,[1] Ayesha Batra,[1] and Robert O. WilliamsIII[1,3]**

*Received 5 November 2013; accepted 10 April 2014; published online 14 May 2014*

***Abstract.*** Recently, inhaled immunosuppressive agents have attracted increasing attention for maintenance therapy following lung transplantation. The rationale for this delivery approach includes a more targeted and localized delivery to the diseased site with reduced systemic exposure, potentially leading to decreased adverse side effects. In this study, the *in vitro* and *in vivo* performance of an amorphous formulation prepared by thin film freezing (TFF) and a crystalline micronized formulation produced by milling was compared for tacrolimus (TAC). Despite the relatively large geometric size, the TFF-processed formulation was capable of achieving deep lung delivery due to its low-density, highly porous, and brittle characteristics. When emitted from a Miat® monodose inhaler, TFF-processed TAC formulations exhibited a fine particle fraction (FPF) of 83.3% and a mass median aerodynamic diameter (MMAD) of 2.26 μm. Single-dose 24-h pharmacokinetic studies in rats demonstrated that the TAC formulation prepared by TFF exhibited higher pulmonary bioavailability with a prolonged retention time in the lung, possibly due to decreased clearance (*e.g.*, macrophage phagocytosis), compared to the micronized TAC formulation. Additionally, TFF formulation generated a lower systemic TAC concentration with smaller variability than the micronized formulation following inhalation, potentially leading to reduced side effects related to the drug in systemic circulation.

**KEY WORDS:** dry powder inhalation; lung bioavailability; lung clearance; micronized; thin film freezing.

## INTRODUCTION

Since 1954, when the first long-term organ transplant was successfully performed, tremendous progress has been made in the field of surgical techniques and transplant medications. The importance of medicines that inhibit the immune system and prevent rejection of a transplanted organ is now better realized. Currently, lung transplantation is the least successful in terms of post-transplant survival rate among all the common solid organ transplants with survival rates of 88% at 3 months, 79% at 1 year, 64% at 3 years, 53% at 5 years, and 31% at 10 years (1). The low survival rate is due to such conditions as bronchiolitis obliterans syndrome (BOS) associated with acute and chronic allograft rejection (1,2). Over the last two decades, immunosuppressive agents have gained more attention in treating rejection after organ and tissue transplantation. Present immunosuppressive therapy consists of a combination of a three orally administered drug regimen, a calcineurin inhibitor (cyclosporine A or tacrolimus), an antimetabolite (mycophenolate mofetil or azathioprine), and a corticosteroid (3).

Cyclosporine A (CsA) and tacrolimus (TAC) are the two most commonly used calcineurin inhibitors for maintenance therapy after organ transplantation (4). CsA was commercialized in 1983 by Novartis under the brand name Sandimmune® for systemic or oral treatment of acute and chronic transplant rejection. TAC, a more potent immunosuppressive drug than CsA (5), can be administered twice daily for maintenance therapy (Prograf®, Astellas). Most recently, an extended release oral formulation of TAC was reported (Astagraf XL®, Astellas) and is taken once daily. It has been reported that TAC improves both short-term graft success and long-term patient survival rates with lower systemic toxicity compared to CsA (6–9). In light of this, TAC is used more frequently than CsA (10). However, the use of TAC is limited by its erratic oral bioavailability (varies from 4% to 93%) and a variety of adverse side effects associated with elevated systemic concentrations over prolonged periods of therapy, such as nephrotoxicity, neurotoxicity, hypertension, diabetes mellitus, and increased risk of opportunistic infection (4).

Another approach to improve clinical outcomes of immunosuppressive agents in lung transplant patients is to administer the drugs via pulmonary inhalation. The rationale for this approach is more targeted and localized delivery with lower systemic exposure related to adverse side effects. Numerous studies reported inhaled CsA formulations to prevent

[1] College of Pharmacy, The University of Texas at Austin, 2409 University Ave. Mail Stop 1920A, Austin, Texas 78712, USA.
[2] Division of Pulmonary Diseases/Critical Care Medicine, Department of Medicine, University of Texas Health Science Center at San Antonio, San Antonio, Texas, USA.
[3] To whom correspondence should be addressed. (e-mail: bill.williams@austin.utexas.edu)

 

rejection after lung transplantation (11–16). One formulation, cyclosporine inhalation solution (CIS) in propylene glycol (300 mg/4.8 mL, administered three times a week), has been investigated and demonstrated positive results (17). Although CIS exhibited no statistical improvements in acute graft rejection compared to inhaled placebo, prevention of chronic rejection and patient survival rates were significantly improved (17). This therapy was denied approval by the U.S. Food and Drug Administration (FDA) due to uncertainties with the carrier vehicle and a lack of clinical efficacy (http://www.fda.gov/ohrms/dockets/ac/05/briefing/2005-4135B1_02_A-FDA-Pulminiq.pdf). Since TAC is more potent than CsA and formulated as a dry powder in the present study, it is possible that inhaled TAC will achieve better clinical outcomes compared to inhaled CsA. Recently, alternative delivery systems containing TAC have been reported for inhalation applications to treat lung diseases, including a metered dose inhaler (18–20), nebulized solution in 70% ethanol (21,22), nebulized nanoparticle dispersions (4,23,24), nanoliposomal dry powder inhalation (25), and respirable low-density brittle matrix particles (26). Similar or slightly enhanced effects (suppression of airway inflammation or prevention of chronic and acute rejection after lung transplantation) and greatly reduced systemic exposure related to potentially decreased side effects were observed for inhaled TAC compared to oral or intramuscular injected TAC. Therefore, inhaled TAC is a feasible approach for maintenance therapy after lung transplantation.

Pulmonary drug delivery by dry powder inhalers (DPIs) has been well established as a valuable and efficient method for local and systemic treatment of diseases. Almost all the marketed DPIs are carrier-based formulations, which have high dose variability and low delivery efficiency (%FPF ranging from 10% to 35%) (26). Recently, engineered particles capable of more efficient pulmonary delivery have gained increasing attention. Large, porous, low-density particles were first introduced by Edwards *et al.*, which are able to achieve deep lung delivery despite their relatively large geometric size (up to 20 μm) (27). Since then, a variety of technologies have been developed to enhance the pulmonary deposition efficiency of DPIs, including AIR® (28), PulmoSphere® (29,30), Technosphere® (31), NanoCluster® (32), and brittle matrix particles prepared by thin film freezing (TFF) (26). Additionally, it has been reported that engineered particles with geometric diameter larger than 10 μm or smaller than 100 nm can escape from macrophage phagocytosis, leading to prolonged lung retention time (33). Moreover, the tailored physicochemical properties of engineered particles (*e.g.* amorphous, enhanced surface area, high porosity, *etc.*) have demonstrated improved drug dissolution rate in the lung lining fluid (4,34). It is generally believed that slow dissolution can be used as a strategy to prolong the drug retention time in the lungs (35). However, undissolved drug particles are more susceptible to mucociliary clearance and macrophage phagocytosis, which will greatly reduce the drug retention (36). Additionally, it has been reported by several researchers that dissolved hydrophobic molecules in the lung lining fluid tend to remain in the lung tissue rather than go to the blood circulation (24,37,38). Hence, it is quite possible that faster dissolution of engineered particles can lead to further prolonged drug retention time in the lungs. Therefore, the TFF process was selected in this study to prepare the TAC formulation suitable for dry powder inhalation which was compared with traditional micronized particles.

Lactose is the only excipient approved by the FDA, which can be used in DPIs at a high amount (up to 25 mg). Nearly all the carrier-based DPI products on the market used lactose as carrier (26). Mannitol (MAN) is also approved by the FDA as an excipient for inhalation, but limited to a very low content (0.051%). However, MAN can be inhaled up to doses of 365 mg (Aridol®, Pharmaxis Ltd.) to assess bronchial hyperresponsivesness in patients. It has been reported by Watts *et al.* that respirable brittle matrix particles prepared by TFF were susceptible to moisture-induced matrix collapse and hygroscopicity when lactose was used as excipient; in contrast, the aerosolization properties of TFF-processed powders with MAN were not influenced by high humidity (26). Therefore, MAN was chosen in this study due to its superior formulation stability.

The objective of this study is to compare the *in vitro* and *in vivo* performance of dry powder inhalation formulations of TAC made by TFF to that made by micronization. We hypothesize that pulmonary delivery of the TFF-processed formulation would yield higher deposition and more prolonged drug retention in the lung, compared to the micronized formulation, due to its aerodynamic properties and differences in clearance. Additionally, the TFF-processed formulation will generate lower systemic concentration with smaller variability compared to micronized formulation, which could possibly lead to decreased side effects. To our knowledge, the pharmacokinetic properties of TAC following dry powder inhalation of amorphous TFF-processed formulation *versus* crystalline micronized formulation have not been previously reported.

## MATERIALS AND METHODS

### Materials

The following materials were purchased: tacrolimus monohydrate (Haroui Pharma-Chem Inc., Irvine, CA); ascomycin (ASCO, LC Laboratories, Woburn, MA); mannitol, HPLC grade acetonitrile, and methanol (Fisher Scientific, Pittsburgh, PA); Polysorbate 80 (Spectrum, Gardena, CA); ethanol (Decon Labs, King of Prussia, PA); 0.9% sodium chloride for injection; and heparin sodium 10,000 units/mL (TW Medical, Lago Vista, TX).

### Preparation of Micronized TACMAN and TFF TACMAN

Micronized TAC powders were prepared by wet ball milling followed by size reduction utilizing jet milling. Two grams of bulk TAC powders (mean particle size 84.7 μm with 100% <127.8 μm, as received from supplier) were dispersed in 25 mL of purified water in a ceramic jar with zirconia grinding media (1/2 in. radius end cylinder) (US Stoneware, East Palestine, OH). The TAC dispersion was milled on a ball mill at 100 rpm under room temperature for 24 h, and the resulting slurry was combined with several successive washings of the ceramic jar and milling media using purified water. The obtained TAC particle dispersion was precooled in a −80°C freezer and lyophilized in a VirTis Advantage bench top tray lyophilizer (The VirTis Company, Inc., Gardiner, NY, USA).

Further size reduction was achieved by feeding the obtained TAC dry powder into an air-jet mill (Aljet mill, Fluid Energy, Plumsteadville, PA, USA) with a feed pressure of 80 psi and a grinding pressure of 65 psi. Samples were collected and analyzed from the collecting chamber. Micronized MAN was produced by jet milling the bulk materials four to five times until the particle size reached the respirable range (1–5 μm). The particle size before and after milling was monitored using a Sympatec Helos laser diffraction instrument (Sympatec GmbH, Germany) equipped with a R3 lens. Briefly, the powder was dispersed in a nonsolvent system (water for TAC, acetone for MAN) by 5 s of sonication. The detector was activated at a minimum optical concentration of between 4% and 5%. Once the desirable size of the TAC and MAN particles were obtained, a physical mixture of micronized TAC and micronized MAN (1:1 by weight, micronized TACMAN) was acquired by blending the two powders using a tubular mixer.

TFF TACMAN was prepared by thin film freezing (TFF) technology. A detailed description of the TFF process was previously reported by Engstrom *et al.* (39). Briefly, MAN was dissolved in purified water and TAC was dissolved in acetonitrile (ACN), respectively. A co-solvent mixture of ACN and water (60:40 *v*/*v*) containing TAC and MAN (1:1 *w*/*w*) was obtained by adequate mixing of the two solutions. The total solid concentration of the co-solvent was 0.75% (*w*/*v*). The co-solvent solution was rapidly frozen on a cryogenically cooled rotating stainless steel surface (−50±3°C). The resulting thin film was removed from the surface by a scraper and maintained in the frozen state in liquid nitrogen. Solvents were sublimated by lyophilization over 48 h at pressures less than 200 mTorr, while the shelf temperature was gradually ramped from −40°C to 25°C. Prior to sample removal from the lyophilizer, dry nitrogen was purged into the chamber to equilibrate to atmospheric pressure and the final product was stored in a vacuum desiccator at room temperature.

### Differential Scanning Calorimetry (DSC)

Thermal properties of micronized TACMAN, TFF TACMAN, and each of their components were determined by a modulated temperature DSC (TA Instruments Model 2920, New Castle, DE) equipped with a refrigerated cooling system. Dry nitrogen gas was purged through the DSC cell at a flow rate of 40 mL/min. Then 5–10 mg of samples were weighed into aluminum crimped pans (Kit 0219-0041, Perkin-Elmer Instruments, Norwalk, CT) and heated at a ramp rate of 10°C/min from 30°C to 250°C with a modulation temperature amplitude of 1°C/60 s. Data were analyzed using TA Universal Analysis 2000 software (TA Instruments, New Castle, DE). TFF TACMAN powders were stored at accelerated condition (30°C/75% RH) for 1, 3, and 6 months, and DSC was conducted to confirm if there is any crystallization of TAC in the composition.

### Powder X-ray Diffraction (PXRD)

The crystallinity of the same set of samples was evaluated by wide angle XRD (A Philips 1710 X-ray diffractometer, Cu Ka1 radiation, $\lambda$=1.54059 Å, 40 kV, 40 mA). Samples were analyzed ranging from 5′ to 40° at a $2\theta$ step size of 0.05° and a dwell time of 2 s.

### Attenuated Total Reflectance-Fourier Transform Infrared Spectroscopy (ATR-FTIR)

Infrared spectra were obtained using a Bruker Equinox55 FTIR spectrophotometer (Karlsruhe, Germany) equipped with a deuterated triglycine sulfate detector and an attached attenuated total reflectance unit (Thermo Scientific, Hudson, NH). The same pressure was applied to all samples against the diamond crystal of the ATR cell by a pressure applicator with a torque knob monitor. Measurements were carried out with a scanning range of 800 to 4,000 $cm^{-1}$, resolution of 4 $cm^{-1}$, and 16 scans per sample. Before each measurement background was scanned and subtracted, all measurements were conducted at least three times to ensure the reproducibility.

### Scanning Electron Microscopy (SEM)

SEM was employed to evaluate the morphology of both micronized and TFF particles. Prior to imaging, samples were mounted under vacuum onto aluminum stages with double-sided carbon tape and coated using sputter coater (Electron Microscopy Sciences, USA) with platinum/palladium targeted for 12 nm thickness. Sample images were captured using a Leo 1530 scanning electron microscope operating at an accelerating voltage of 10 kV.

### Brunauer–Emmett–Teller (BET) Specific Surface Area Analysis

Specific surface area was determined by a Monosorb MS-21 surface area analyzer. The Monosorb utilizes a modified BET equation for extremely rapid, single-point determinations of surface area ($P/P_0$=0.294). Samples were degassed at 30°C by nitrogen purging (20 psi) for at least 2 h prior to measurement, and 30% nitrogen in helium was used as the adsorbate gas.

### Geometric Particle Size Measurement

Geometric particle size of micronized TACMAN and TFF TACMAN aerosolized from a Miat monodose inhaler® (Miat, Milan, Italy) was measured by low angle light scattering technique using a Malvern Spraytec® (Malvern, UK) equipped with an inhalation cell and an induction port. The inhaler was loaded with a size 3 hypromellose (HPMC) capsule (Capsugel, Peapack, NJ) containing 3 mg of formulation and fitted to the mouth of the induction port by a silicone adapter. A predetermined flow rate of 90 L/min to achieve a 4-kPa pressure drop across the device was used for all measurements (40). Data were collected over 4 s upon actuation when laser transmission dropped below 98%. Values reported are the average of at least three measurements.

### *In Vitro* Aerosol Performance

The aerodynamic properties of TFF TACMAN were investigated by a Next Generation Impactor (NGI) (MSP Corp., Shoreview, MN). A similar setup with the geometric particle size measurement was used. The Miat monodose inhaler® loaded with size 3 HPMC capsules containing 3 mg of formulation was secured to the induction port by a silicone

adapter. Aerosols were generated over 2.7 s at a flow rate of 90 L/min to achieve an inhalation volume of 4 L. Prior to actuation, surfaces of collection stages were coated with 1% polysorbate 80 in ethanol (*v*/*v*) and allowed to completely dry, as recommended by the European Pharmaceutical Aerosol Group (EPAG) (41). The cut-off size for each stage was calculated to be 6.48, 3.61, 2.30, 1.37, 0.76, 0.43, and 0.26 μm from stages 1 to 7 and micro-orifice collector (MOC), respectively (42). Following actuation, the deposited powders in the capsule, inhaler, adaptor, induction port, stages 1 to 7, and MOC were collected by rinsing each area with 10 mL of methanol/water (90:10, *v*/*v*), which is the mobile phase for TAC quantification (43). Briefly, TAC content was analyzed using a Dionex high performance liquid chromatography (HPLC) system equipped with a reversed phase C18 column (150 mm×4.6 mm, 5 μm, 300 Å) with a Universal security guard column (Phenomenex, Torrance, CA). The mobile phase consisted of 90:10 (*v*/*v*) methanol/water and the injection volume was 20 μL. TAC was eluted over 6 min at a flow rate of 0.8 mL/min and a detection wavelength of 210 nm.

The emitted dose (ED) was calculated as the percentage of drug emitted from the inhaler with respect to the total loaded dose into the capsule. The mass median aerodynamic diameter (MMAD), geometric standard deviation (GSD), and fine particle fraction (FPF) were calculated according to the USP 32-NF 27 General Chapter 601 (44). A plot of cumulative percentage of mass less than the stated aerodynamic diameter *versus* aerodynamic diameter (cut-off size for each stage) was built and fit to a four-parameter logistic curve using Sigmaplot (Systat Software Inc., San Jose, CA). MMAD and GSD were calculated based on the drug deposition from stages 1 to 7 and MOC. FPF was determined as the percentage of aerosolized particles with a MMAD less than 5 μm with respect to the emitted dose.

### *In Vivo* Pulmonary Dosing in Rats

*In vivo* pharmacokinetic study was conducted using Sprague–Dawley rats (Charles River Laboratories, Inc., Wilmington, MA) in compliance with the Institutional Animal Care and Use Committee (IACUC) guidelines at The University of Texas at Austin. The rats (male and female: weighing from 250 to 300 g with an average weight of 270 g) were housed in a 12-h light/dark cycle with access to food and water *ad libitum*. Rats were subjected to 1 week of acclimation time to the housing environment and another week of restraint training in the nose-only dosing chamber. Powder aerosols were generated by a rotating brush generator (Palas RBG 1000, Palas GmbH, Karlsruhe, Germany). A detailed setup of the dosing apparatus was illustrated in Fig. 1. Sixteen rats were dosed for each formulation group (12 non-precatheterized rats for lung sample collection and four precatheterized rats for blood sample collection). Prior to dosing, the exposure time for micronized TACMAN and TFF TACMAN was calculated to ensure that the same TAC concentrations in the chamber were achieved. After exposure to the aerosolized powders, blood samples were withdrawn from a jugular vein catheter at 0.25, 1, 2, 4, 8, 12, and 24 h and stored in a BD Vacutainer® blood collection tube at −80°C until analyzed. Equivalent volume of saline was replaced after each withdrawing. Three rats from each group were sacrificed at each time point (0.5, 1, 2, 8, and 24 h) and lung samples were obtained. Prior to the lung sample collection, a modified bronchoalveolar lavage (BAL) procedure was performed (25). Briefly, the trachea was exposed by blunt dissection of the sternohyoideus muscle, and a small incision was made to insert the lavage needle outfitted with a 5-mL BD syringe. Approximately 3 mL of sterile phosphate buffered saline (PBS) was slowly injected to fill the lungs and the BAL fluid was withdrawn by gentle aspiration. This procedure was conducted twice so the total yield of BAL was between 4 and 5 mL. Then the lung was excised and stored in a −80°C freezer prior to analysis.

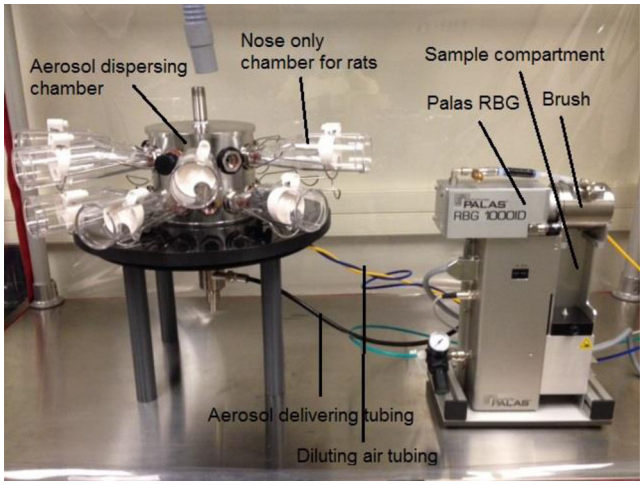


**Fig. 1.** Illustration of RBG and nose-only dosing apparatus for rats

### Quantification of TAC Concentration in the Lung and Blood

TAC concentration in the lung and blood was quantified by liquid chromatography mass spectrometry (LC/MS/MS). The LC/MS/MS system consisted of a Shimadzu SCL-10A Controller, LC-10AD pump with a FCV-10AL mixing chamber, SIL-10AD autosampler, and an AB Sciex API 3200 tandem mass spectrometer with turbo ion spray. The analytical column (Grace Alltima C18, 4.6×150 mm, 5 μm, Alltech, Deerfield, IL) was maintained at 60°C during the chromatographic runs using a Shimadzu CTO-10A column oven. Mobile phase A contained 10 mM ammonium formate and 0.1% formic acid dissolved in HPLC grade methanol. Mobile phase B contained 10 mM ammonium formate and 0.1% formic acid dissolved in 90% HPLC grade methanol. The flow rate was maintained at 0.5 mL/min and TAC was eluted with a step gradient. The column was equilibrated with 100% mobile phase B. At 6.1 min after injection, the system was switched to 100% mobile phase A. Finally, at 15.1 min, the system was switched back to 100% mobile phase B in preparation for the next injection. The TAC transition was detected at 931.6 Da (precursor ion) and the daughter ion was detected at 864.5 Da. ASCO (internal standard) was detected at 809.574 Da and the daughter ion was 756.34 Da. The ratio of the peak area of TAC to that of the internal standard (response ratio) for each unknown sample was compared against a linear regression of calibrator response ratios to quantify TAC.

For extraction of TAC from whole blood sample, 100 μL of calibrator and unknown whole blood samples were mixed with 10 μL of 0.5 μg/mL ASCO (internal standard), 300 μL of

a solution containing 0.1% formic acid, and 10 mM ammonium formate dissolved in 95% HPLC grade methanol. The samples were vortexed vigorously for 2 min and centrifuged at 15,000*g* for 5 min. The supernatants were transferred to 1.5 mL microfilterfuge tubes and centrifuged at 15,000*g* for 1 min and then 40 μL of the final extracts were injected into the LC/MS/MS system. The concentration of TAC was expressed as nanograms per milliliter in the whole blood.

TAC was extracted from rat lung tissue according to the following protocol. Briefly, 100 mg of calibrator, control, and unknown tissue samples were mixed by sonication (three 5 s bursts) with 10 μL of 0.5 μg/mL ASCO (internal standard) and 300 μL of a solution containing 0.1% formic acid and 10 mM ammonium formate dissolved in 95% HPLC grade methanol. After sonication, the samples were vortexed vigorously for 2 min, and then centrifuged at 15,000*g* for 5 min. The supernatants were transferred to 1.5 mL microfilterfuge tubes and centrifuged at 15,000*g* for 1 min and then 40 μL of the final extracts were injected into the LC/MS/MS. The concentration of TAC was expressed as nanograms per gram in the lung tissue.

### Pharmacokinetic and Statistical Analysis

Plots of the concentration of TAC in the lung tissue and whole blood *versus* time were used to compare the pharmacokinetic behaviors of micronized TACMAN and TFF TACMAN. The TAC concentration at the first time point (0.5 h) was considered as the initial dose. The TAC concentrations in the lung were normalized with respect to the TAC concentration at the first time point (0.5 h) and expressed as the percentage of initial concentration measured in the lung. A two-compartmental model was selected to calculate the pharmacokinetic parameters of TAC in the rat lung with the assistance of WinNonlin Professional Version 2.1 (Pharsight Corporation, Mountain View, CA). The area under the concentration *versus* time curve ($AUC_{0-24\ h}$) was calculated by the linear trapezoidal rule using average TAC concentrations in the lung. Student's *t* tests were conducted to determine the significance between the two dosing groups. For all tests, statistical significance was defined by $p \leq 0.05$.

## RESULTS AND DISCUSSION

### Crystallinity

DSC was used to evaluate the thermal properties of micronized TACMAN, TFF TACMAN, and their individual components (Fig. 2). Micronized TAC displayed a melting peak at 127.16°C and an enthalpy of fusion of 32.11 J/g; micronized MAN exhibited a melting peak at 171.17°C and an enthalpy of fusion of 292.8 J/g, indicating that both components are crystalline after micronization. Both of the melting peaks of TAC and MAN were present in micronized TACMAN (1:1). For 1 g of micronized TACMAN (1:1), there were 0.497 g of TAC and 0.503 g of MAN, so the enthalpy of fusion for TAC endothermic peak based on the mass of TAC in micronized TACMAN (1:1) equals to 16.16/0.497 J/g, namely 32.52 J/g, which was very similar to the experimentally determined enthalpy of fusion of micronized TAC alone. Hence, nearly 100% of the TAC in micronized TACMAN (1:1) was crystalline (45). Similarly, the enthalpy of fusion for MAN endothermic peak based on the mass of MAN in micronized TACMAN (1:1) equals 149.8/0.503=297.8 J/g, which correlated to the enthalpy of fusion in micronized MAN alone, indicating 100% of the MAN in micronized TACMAN (1:1) was crystalline as well. TFF TAC only (no excipients, 100% potency) displayed a single glass transition temperature ($T_g$) of TAC at 75.42°C. TFF MAN only exhibited an endothermic melting peak of MAN with an enthalpy of fusion (280.2 J/g) very close to the enthalpy of fusion of micronized MAN alone (292.8 J/g), meaning that the MAN in TFF MAN only was nearly 100% crystalline. In the TFF TACMAN (1:1) DSC profile, there was a single $T_g$ (76.28°C) corresponding to the $T_g$ of TAC (75.42°C) and no melting peak of TAC was detected, indicating the TAC in TFF TACMAN was amorphous; there was also an endothermic melting peak at 167.75°C corresponding to the melting of MAN (169.09°C) with an enthalpy of fusion of 138.2 J/g. Based on the potency (50.7%) of MAN in TFF TACMAN (1:1), the enthalpy of fusion for MAN endothermic peak based on the mass of MAN in TFF TACMAN (1:1) is equal to 138.2/50.7%=272.6 J/g, similar to the melting of MAN alone; therefore, the MAN in TFF TACMAN (1:1) was 100% crystalline. In summary, TAC and MAN exhibited amorphous and crystalline properties, respectively, in TFF TACMAN (1:1). As illustrated in Fig. 3, when TFF TACMAN powders were stored at accelerated condition (30°C/75% RH) for 1, 3, and 6 months, there was still no melting peak of TAC, and the $T_g$ of TAC was about 76°C at each time point. Therefore, TFF TACMAN is stable up to 6 months in terms of the amorphicity of TAC.

In the XRD diffraction pattern (Fig. 4), TAC exhibited intense characteristic crystalline peaks at 8.55, 12.75, 13.85, 14.25, 15.4, and 19.85 2-theta degrees in the micronized TAC, distinguished from the crystalline peaks of MAN at 14.7, 16.85, 18.85, 20.5, 21.15, 24.65, and 36.1 2-theta degrees in micronized MAN. Micronized TACMAN (1:1) had both the characteristic peaks of TAC and MAN, indicating that both TAC and MAN were crystalline in micronized TACMAN (1:1). All of the characteristic peaks of TAC disappeared in TFF TAC only, indicating a highly amorphous morphology of TAC molecules (46). In the TFF MAN only XRD profile, some of the characteristic peaks of MAN disappeared and the intensity of some peaks has been greatly reduced. It has been reported that the reduction of XRD peak intensity and broad halo peaks may be attributed to the reduction of particle size or change in crystalline microstructure (47). As seen in the SEM images (Fig. 5), TFF-produced formulations exhibited a highly porous structure. Although it was not a complete particle size reduction due to aggregation if discrete particles are considered, the large pores between particles may cause molecules to lose their long-range crystalline order but still not be amorphous (47). Therefore, the MAN in TFF MAN only exhibited crystalline properties. TFF TACMAN (1:1) displayed no characteristic crystalline peaks of TAC, but some broaden and intensity-reduced peaks of MAN corresponding to the peaks in TFF MAN only. Hence, the TAC in TFF TACMAN (1:1) was amorphous and MAN was crystalline.

According to the DSC and XRD results, the crystalline state of TAC and MAN can be predicted during the entire manufacturing process. Initially, TAC was dissolved in

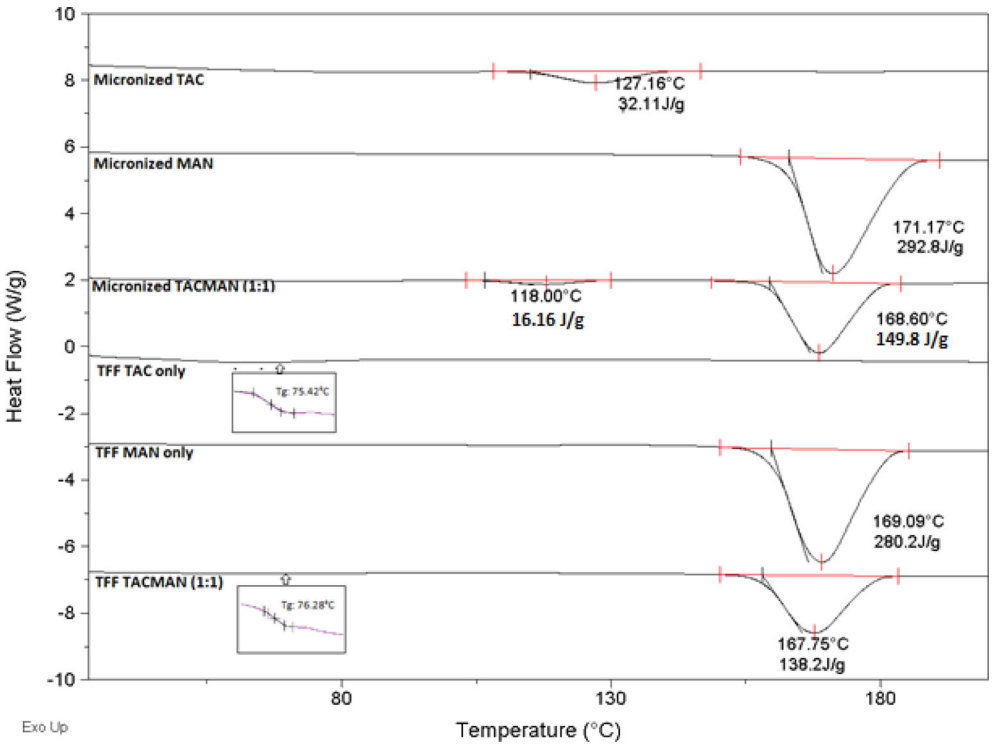


**Fig. 2.** DSC profiles of (from *top* to *bottom*) micronized bulk TAC, micronized bulk MAN, physical mixture of micronized TAC and MAN (1:1), TFF TAC only, TFF MAN only, and TFF TACMAN (1:1)

acetonitrile (ACN) and MAN was dissolved in water. TAC molecules and MAN molecules were homogenously dispersed in the co-solvent composed of ACN and water due to the high miscibility of ACN and water. During the TFF process, TAC and MAN are capable of transitioning into a glassy amorphous state because the extremely rapid cooling rate (estimated to be $10^6$ K/s) can prevent the nucleation and growth of crystals (46). Then during the lyophilization process, TAC remained amorphous due to its high $T_g$ (75.42°C); MAN started to crystallize at its $T_g$ (13°C,

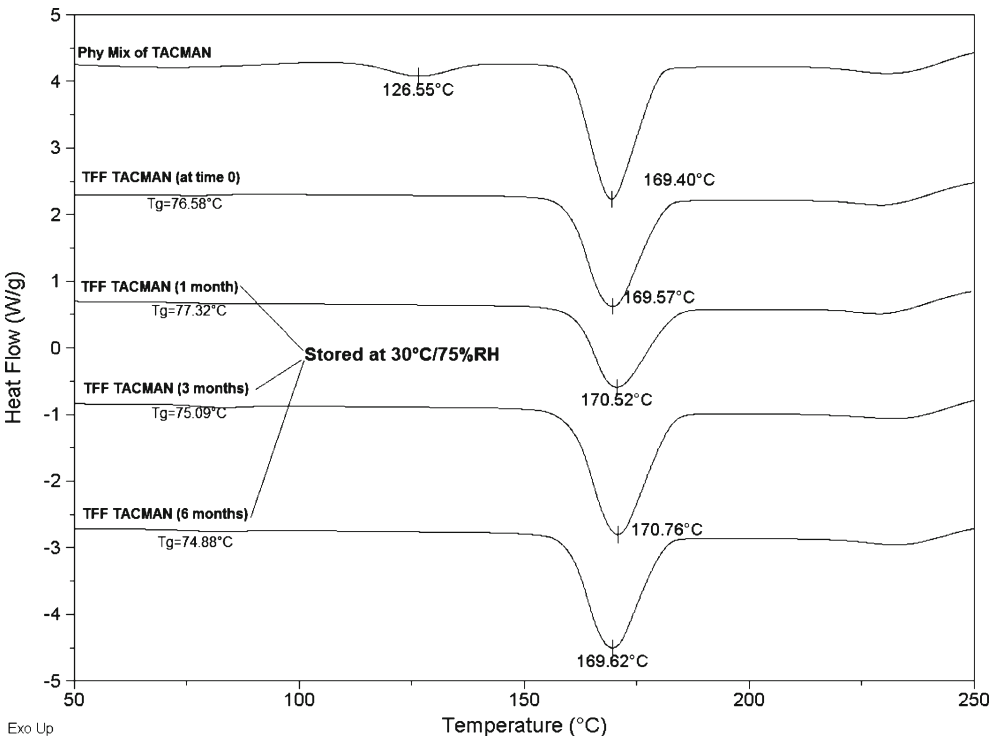


**Fig. 3.** DSC of TFF TACMAN stored at 30°C/75% RH at time 0, 1 month, 3 months, and 6 months

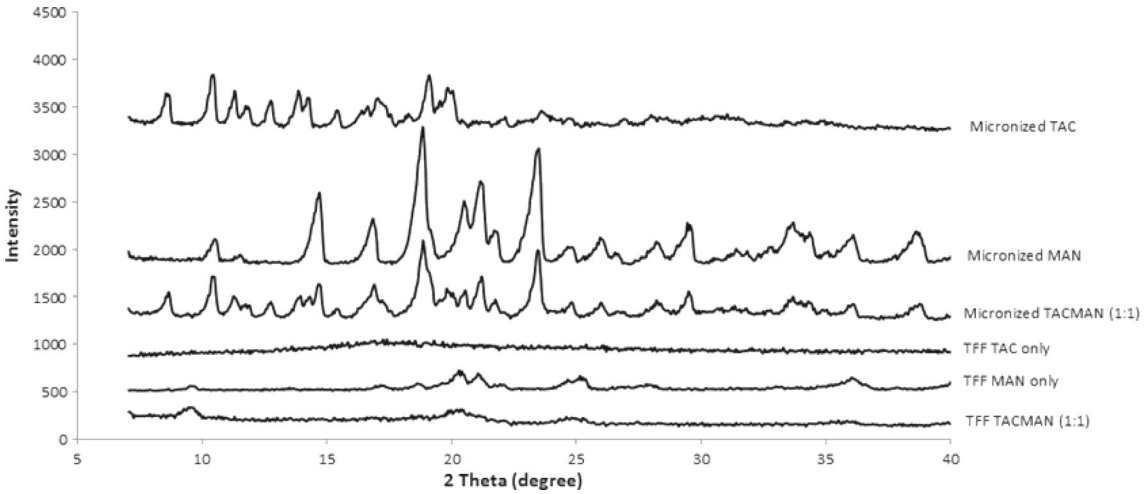


**Fig. 4.** X-ray powder diffraction patterns (from *top* to *bottom*): micronized bulk TAC, micronized bulk MAN, physical mixture of micronized TAC and MAN (1:1), TFF TAC only, TFF MAN only, and TFF TACMAN (1:1)

measured from quench-cooled melt (48)). It has been reported that with a second component added into the MAN solution, the relative concentration threshold above which MAN will crystallize during the lyophilization process is about 30% (*w*/*w*), and this ratio is largely independent of the nature of the second solute (48). In our case, TAC was considered as the second solute and the weight ratio of MAN in the formulation is about 50% (*w*/*w*); therefore, MAN was still crystalline after being freeze-dried. The seeding of crystalline MAN did not have an impact on TAC molecules because there is no interaction between TAC and MAN molecules according to the ATR-FTIR results (data

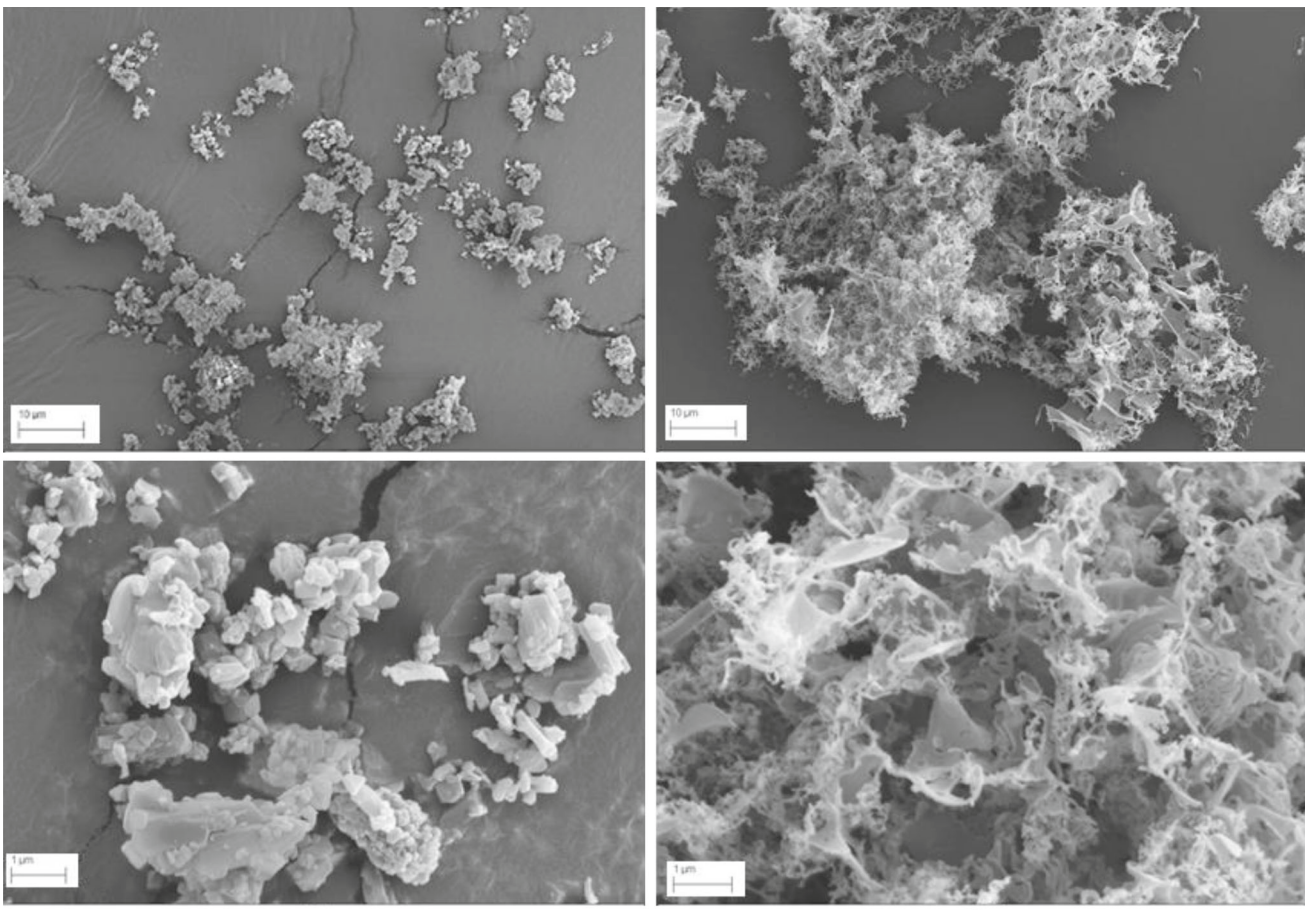


**Fig. 5.** SEM images of micronized TACMAN (**a**) and TFF TACMAN (**b**) under different magnifications: *top* (2.70KX, *scale bar*=10 μm) and *bottom* (25.00KX, *scale bar*=1 μm)

shown in Fig. 6; explanation follows below). Consequently, the final product, TFF TACMAN (1:1), consists of both amorphous TAC domains and crystalline MAN domains.

### Molecular Interactions Investigated by ATR-FTIR

ATR-FTIR was conducted in order to investigate the molecular interactions between TAC and MAN (Fig. 6). The micronized TAC spectrum exhibits absorption bands of C=C stretch at 1,638 $cm^{-1}$ and resonating amidic C=O and ketonic C=O stretching vibrations at 1,740, 1,728, and 1,693 $cm^{-1}$, which can be distinguished from the spectrum of micronized MAN with a broad OH stretch peak only (49). In the micronized TACMAN (1:1) spectrum, all these bands were observed with the same absorbance, indicating that there were no interactions between TAC and MAN molecules that existed in this physical mixture of micronized TACMAN. However, in the spectrum of TFF TAC only, the band of C=C stretch shifted from 1,638 to 1,650 $cm^{-1}$, and the bands of resonating amidic C=O and ketonic C=O stretching vibrations shifted from 1,740, 1,728, and 1,693 to 1,746, 1,716, and 1,684 $cm^{-1}$, respectively. It has been reported that the absorbance of FTIR peaks is very sensitive to the crystal-packing configuration of different forms (50). Accordingly, the shiftiness of TAC absorption peaks in TFF TAC only was attributed to the state change from crystalline to amorphous. The same absorption peaks were observed in TFF TACMAN (1:1) compared with TFF TAC only, indicating that there was no interaction between TAC and MAN molecules in TFF TACMAN. In summary, there is no evidence from the spectra of any hydrogen bond interactions between tacrolimus and mannitol in either the micronized formulation or TFF formulation.

### Morphology, Geometric Particle Size, and Aerodynamic Properties

Micronization was employed to physically reduce the particle size and maintain their original crystalline structure. Dry milling in a fluid energy mill (*e.g.*, air-jet mill) is a typically used micronization technique. Despite the high energy input for jet milling, the process is extremely rapid and the materials are subjected to limited thermal stress (51). However, the major issue with jet milling is the relatively low yield and loss of valuable materials during the repeated feeding and discharging compared to other milling techniques (52). Low energy wet ball milling is another widely used micronization technique. Theoretically, the yield from a wet ball milling process can reach up to 100%, but this micronization process requires a long time (hours to days) due to the low energy input (51). Therefore, a combination of wet ball milling and jet milling was employed in the present study to achieve a high yield of micron-size drug particles and shorten the processing time.

For pulmonary drug delivery, the optimum particle size is 1–5 μm (53). In the present study, the mean particle size of TAC was reduced from 84.7 μm (bulk unprocessed TAC as received from supplier) to 8.6 μm (ranging from 1.5 to 22.8 μm) by wet ball milling for 24 h. No further size reduction was observed for longer milling times (up to 1 week) because the milling efficiency not only depends on the processing time, but it is also controlled by other parameters, such as the hardness of the material, nature of the milling medium, and the wetting of the solids (34). Following nonsolvent removal by lyophilization, the size of the TAC particles was further reduced by feeding the dry TAC powders processed from wet ball milling to a jet mill. After one run on the jet mill, the mean

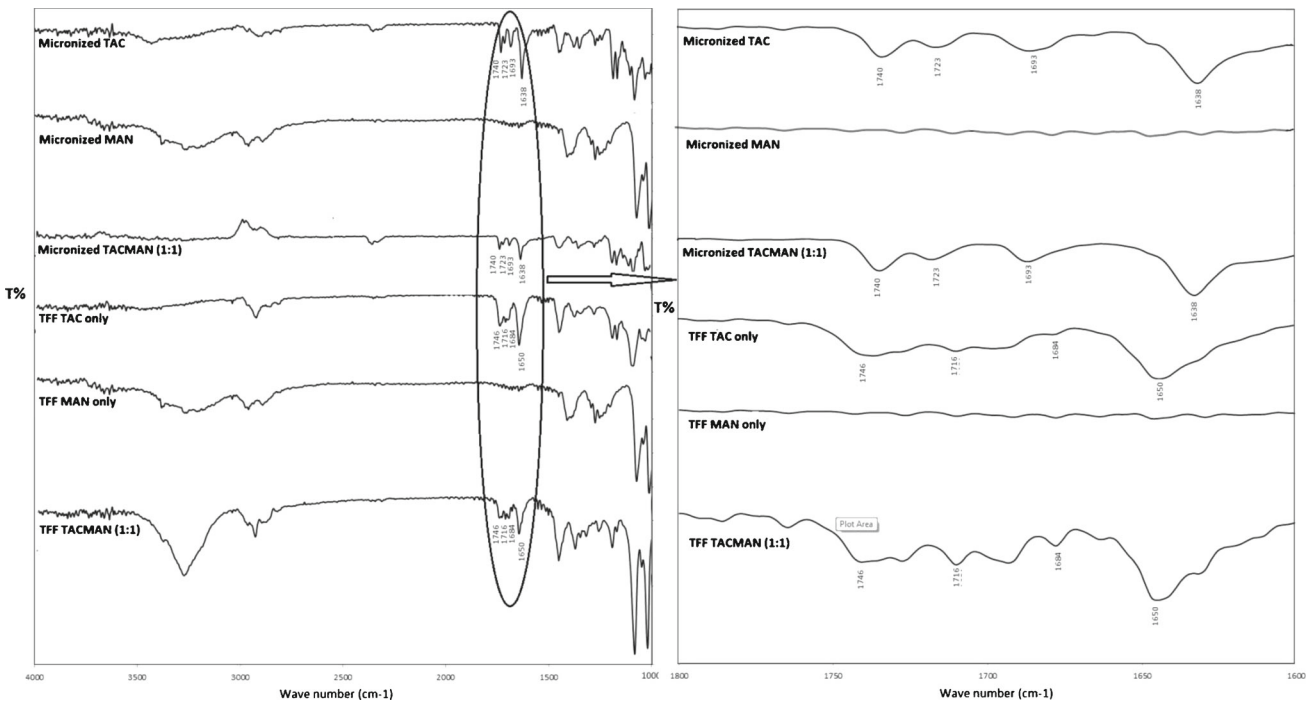


**Fig. 6.** Attenuated total reflectance-Fourier transform infrared spectroscopy of (from *top* to *bottom*): micronized bulk TAC, micronized bulk MAN, physical mixture of micronized TAC and MAN (1:1), TFF TAC only, TFF MAN only and TFF TACMAN (1:1)

particle size of TAC particles decreased from 8.6 μm (D10= 1.5 μm, D90=22.8 μm) to 3.4 μm (D10=1.1 μm, D90=7.4 μm). Mannitol was micronized only by jet milling. After three to four runs on the jet mill, the particle size distribution of MAN was reduced to approximately the same size as the micronized TAC (D10=1.1 μm, D50=3.2 μm, D90=7.0 μm). The potency of TAC in micronized TACMAN (1:1) was 49.7%, indicating that adequate mixing was achieved and the mixture of micronized TAC and MAN is homogenous.

From the SEM images shown in Fig. 5a, micronized TACMAN (1:1) is composed of fractured, irregular shaped particles with a wide size range and a large portion of particle agglomerates due to their cohesive behavior from electrostatic charge generated during the milling process (54). On the other hand, TFF TACMAN (1:1) exhibited a highly porous structure composed of aggregated particle networking, in which discrete particles are barely distinguishable, as displayed in Fig. 5b. The specific surface area of micronized TACMAN and TFF TACMAN was 2.87 and 32.45 $m^2/g$ (Table I), respectively.

From a formulation perspective, the efficacy of drugs administered by pulmonary delivery is largely determined by the aerodynamic diameter of the aerosol particles (53). In general, the optimum aerodynamic diameter for achieving deep lung deposition is 1–3 μm (55). The aerodynamic properties of TFF TACMAN were described in terms of the ED, MMAD, GSD, and FPF of the emitted dose, as illustrated in Fig. 7. TFF TACMAN was capable of emitting 94.2% of the loaded dose from the device, because of the low-density and highly porous structure of TFF particles, and the turbulent airflow readily entered into the large pores to shear the aggregated particles apart and emit them from the device. The FPF and MMAD of TFF TACMAN were 83.3% and 2.26 μm, respectively, indicating that the shear and impaction forces generated by the air flow and the device were able to break the TFF brittle matrix particles into respirable low-density microparticles (26). In addition, ED×FPF represents the percentage of total emitted dose that can achieve deep lung delivery; in this study, up to 78.5% of the TFF TACMAN can be delivered to the lung using Miat® Monodose inhaler. GSD gives an indication of the polydispersity of an aerosol particle size distribution; TFF TACMAN had a relatively small aerodynamic size distribution with a GSD of 2.08 μm. From the results obtained, we can conclude that TFF TACMAN is suitable for deep lung delivery when incorporated into a commercially available DPI.

Besides the aerodynamic diameter, geometric particle size also plays an important role in determining the fate of aerosol particles in the lung. It is well known that the two main clearance mechanisms active in the lung are mucociliary clearance (MCC) in the central and small airways and macrophage phagocytosis in the alveolar region (56). Particles with a geometric size larger than 6 μm are usually cleared by MCC in the ciliated region of the lung (35) and particles with diameters between 1 and 5 μm are preferably engulfed by alveolar macrophages in the alveoli (33). The geometric size distribution of emitted aerosol particles was measured by laser diffraction following aerosol generation from the Miat® monodose inhaler. Micronized TACMAN exhibited a polydispersed size distribution with D10, D50, and D90 (diameter at which the cumulative sample volume was less than 10%, 50%, and 90%) values of 0.93, 1.92, and 4.82 μm, respectively. On the other hand, aerosolized TFF TACMAN had a significantly larger geometric size (shown in Table I, D10= 4.39 μm, D50=17.84 μm, D90=64.49 μm). The aerodynamic diameter is calculated by the following equation:

$$D_{ae} = D_{eq}\sqrt{\rho_p/\rho_0 X}$$

where $D_{eq}$ is the geometric diameter of the particle, $\rho_p$ is the particle density, and $X$ is the dynamic shape factor derived from a sphere. Hence, the aerodynamic diameter is not only dependent on geometric size, but also controllable by the particle density and shape. In the case of TFF TACMAN, assuming the shape of aerosolized particles is spherical, the calculated particle density is 0.016 $g/cm^3$. Therefore, micronized TACMAN is likely to be cleared by macrophage phagocytosis when they reach the alveolar region due to their geometric size (1.92 μm); by contrast, TFF TACMAN particles have the potential to escape from macrophage uptake while achieving deep lung delivery due to their relatively large geometric size (17.84 μm) and small aerodynamic diameter (2.26 μm).

### Pharmacokinetic Analysis of Micronized TACMAN *Versus* TFF TACMAN

The *in vivo* performance of inhaled micronized TACMAN and TFF TACMAN was investigated in a rat model. Rats were exposed via nose-only administration to aerosolized powders generated by a rotating brush generator (RBG). The delivered dose is calculated according to the equation below:

$$DD = C \times RMV \times D$$

where DD is the delivered dose (mg), $C$ is the concentration of substance in air (mg/L), RMV is the respiratory minute volume (*i.e.*, the volume of air inhaled in one minute, L/min), and $D$ is the exposure duration (min). The RMV for rats is calculated according to the formula: RMV (L/min)= $0.608 \times BW\ (kg)^{0.852}$, where BW represents the body weight of the tested subjects (57). Of the delivered dose, only a small percentage will actually deposit in the lungs. The deposition

**Table I.** Specific Surface Area (SSA) and Geometric Particle Size Distribution of Micronized TACMAN (1:1) and TFF TACMAN (1:1). Values Are Expressed as Mean±SD ($n$=3)

| | | | Geometric particle size (μm) | | |
|---|---|---|---|---|---|
| | TAC potency (%) | SSA ($m^2/g$) | D10 | D50 | D90 |
| Micronized TACMAN (1:1) | 49.7 | 2.87±0.16 | 0.93±0.03 | 1.92±0.05 | 4.82±0.08 |
| TFF TACMAN (1:1) | 50.3 | 32.45±3.28 | 4.39±0.21 | 17.84±0.57 | 64.49±2.89 |

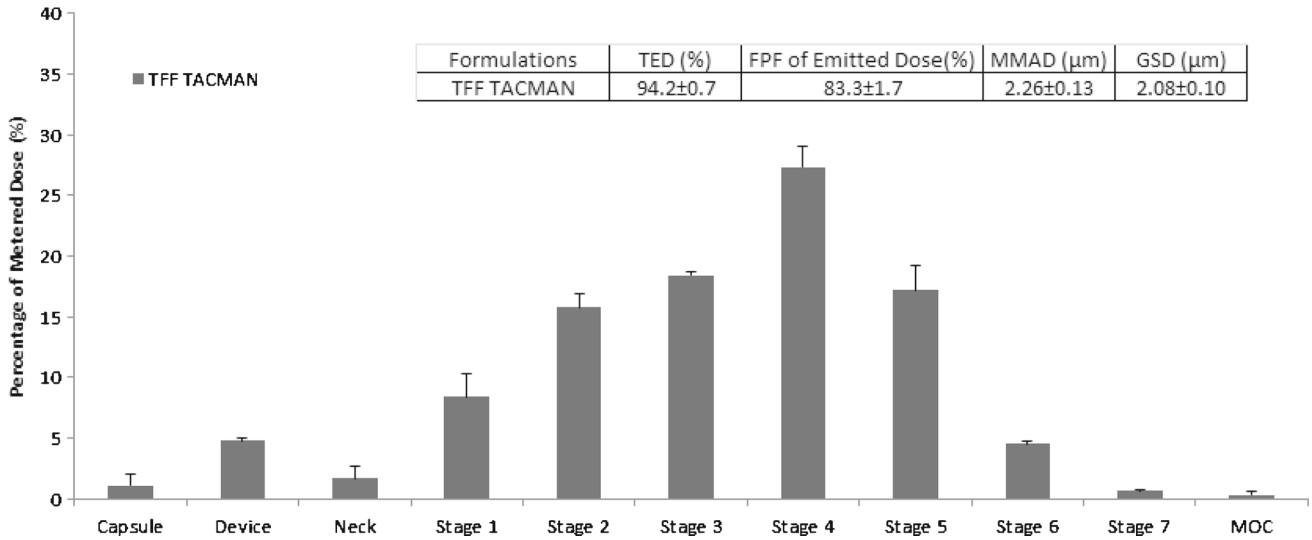


| Formulations | TED (%) | FPF of Emitted Dose(%) | MMAD (μm) | GSD (μm) |
|---|---|---|---|---|
| TFF TACMAN | 94.2±0.7 | 83.3±1.7 | 2.26±0.13 | 2.08±0.10 |

**Fig. 7.** Aerodynamic diameter distribution of TFF TACMAN when emitted from a Miat® monodose inhaler at a flow rate of 90 L/min

fraction of the delivered dose in rats typically ranges between 10% and 5% of the delivered dose and has been shown to be dependent on particle size distribution (58).

Following exposure of the aerosolized powder, a 24-h pharmacokinetic profile was determined in lung tissue and blood for micronized TACMAN and TFF TACMAN. For comparison purposes, TAC concentrations in the lung were normalized with respect to the concentration at the first time point (0.5 h) and expressed as a percentage of initial doses (%) and determined as a function of time (Fig. 8). The TAC concentrations in the lung at 0.5 h were 265.8 ng/g for TFF TACMAN and 122.6 ng/g for micronized TACMAN. A two-compartment model (Fig. 9) was used to calculate the PK parameters in the lung for micronized TACMAN and TFF TACMAN and the results are shown in Table II. The two-compartment model was chosen because it best described the PK behavior of inhaled drug. Following single-dose inhalation, drug particles are deposited along the entire airway so the lungs are considered as the main compartment. Dissolved drug molecules in the lungs can be absorbed into the systemic circulation while undissolved drug particles are eliminated by multiple lung clearance mechanisms. After the drug molecules are absorbed into the blood circulation, they can be re-absorbed from the blood into the lungs. Moreover, they can be transferred to other organs or eliminated from the body. Additionally, the two-compartment model best fit the observed data when the lung and blood data modeled simultaneously.

In the model, the rate constant K10 describes the lung clearance rate, which represents a combination effect of mucociliary clearance, macrophage phagocytosis, and metabolism. K12 and K21 are exchange rates of drug between the lung and the blood compartments. As seen in Table II, K10 of micronized TACMAN (2.64 $h^{-1}$) is approximately 4.7 times greater than that of TFF TACMAN (0.56 $h^{-1}$), indicating that the lung clearance rate is much faster for micronized particles compared to aerosolized TFF particles. Micronized TACMAN exhibited faster clearance rate because most of the particles tend to be engulfed by macrophages due to the phagocytic favorable geometric size (mean 1.92 μm); in contrast, TFF TACMAN had a relatively large geometric particle size (mean 17.84 μm). Based on estimations from macrophage uptake studies, it could be predicted that more than 90% of the TFF particles are capable of escaping clearance from macrophage phagocytosis (59). It is also possible that TFF particles undergo rapid dissolution, leaving little to be cleared by mucociliary clearance and macrophages compared to the more kinetically stable crystalline particles (4,23). The dissolved TAC molecules from TFF particles quickly diffused into the lung tissue, while the undissolved micronized

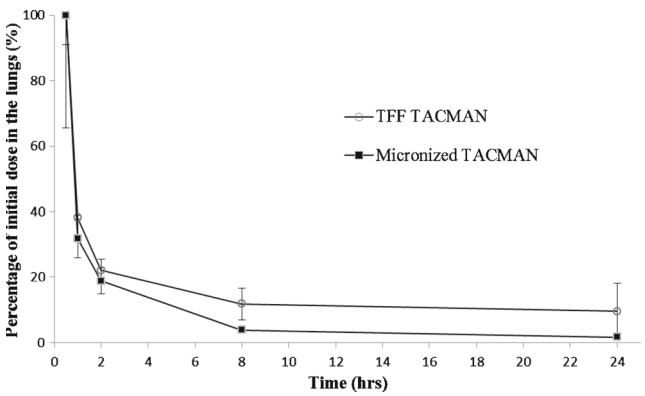


**Fig. 8.** TAC concentration in the rat lungs plotted as percentage of initial dose following exposure to dry powder aerosols generated from a rotating brush generator. TFF TACMAN (*open cycle*) and micronized TACMAN (*solid square*)

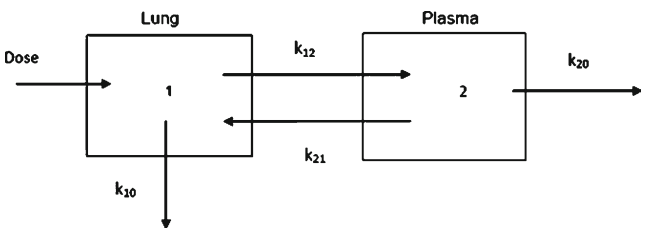


**Fig. 9.** Two-compartment model for determination of lung pharmacokinetic parameters

**Table II.** Lung Pharmacokinetic Parameters of TFF TACMAN (1:1) and Micronized TACMAN (1:1) Following Single-Dose Exposure to Dry Powder Aerosols Generated from a Rotating Brush Generator. All the Parameters Were Calculated Based on Average Lung Concentration ($n=5$)

| Pharmacokinetic parameters | TFF TACMAN (1:1) | Micronized TACMAN (1:1) |
|---|---|---|
| $AUC_{0-24h}$(ng h/g) | 1,707.47 | 729.53 |
| K10 ($h^{-1}$) | 0.56 | 2.64 |
| K12 ($h^{-1}$) | 2.16 | 1.70 |
| K21 ($h^{-1}$) | 0.20 | 0.45 |
| $C_{max}$ (ng/g) | 948.20 | 1,924.83 |
| CL (ng/(h ng/g)) | 2.93 | 6.85 |
| MRT (h) | 21.18 | 1.82 |
| Model fit ($R^2$) | 0.9985 | 0.9999 |

*AUC* area under the concentration–time curve, *CL* clearance rate, *MRT* mean residence time

TAC particles were cleared out of the lungs. Therefore, TFF particles exhibited longer retention time in the lungs than micronized particles. The lung clearance trends observed from the two formulations differ significantly from 2 to 8 h. This difference is supported by prior macrophage clearance studies where 50–75% of the micron-size particles are cleared by macrophages by 2–3 h and 90% or more by 10 h (60).

The systemic absorption rate of TAC from the lung epithelium (K12) is slightly higher for TFF TACMAN (2.16 $h^{-1}$) compared to micronized TACMAN (1.70 $h^{-1}$). According to Fick's first law, K12 is proportional to the membrane permeability, surface area over which the drug is deposited and the drug concentration in the lung lining fluids. In humans, deposition of particles less than 3 μm is thought to occur predominately in the deep lung. Kuehl *et al.* showed that in mice and rats, particles with different mean sizes (0.5, 1, 3, 5 μm) deposited along the entire airway including oral/nasal, trachea/bronchi, and lungs (58). In the present study, the aerodynamic size distribution of the aerosol generated by the RBG was very similar for TFF TACMAN and micronized TACMAN (with MMAD values measured at about 1.5 μm). Hence, the regional deposition pattern should be comparable for the two formulations. Accordingly, the drug permeability due to regional deposition should be similar for both formulations. Drug permeability, however, may not be the same in both formulations due to differences in physicochemical properties described earlier. It has been reported that amorphous TAC can reach up to 10 times supersaturated solubility compared to crystalline TAC (4). These *in vitro* studies provided evidence that TFF TACMAN dissolved more rapidly and to a greater extent than the micronized blend in this study. Additionally, the faster dissolution rate of amorphous TFF TACMAN may make it less susceptible to mucociliary clearance since the drug is rapidly dissolved and able to permeate into airway tissues. All of the effects mentioned above could contribute to enhanced pulmonary bioavailability of TFF TACMAN. If we normalize the data by assuming that the same dose was delivered in both groups, the average $AUC_{0-24\ h}$ in the lung is 1,707.47 and 729.53 ng h/g for TFF TACMAN and micronized TACMAN, respectively. Once the TAC dissolves in the lung lining fluid, it is available for absorption and will either remain in the pulmonary tissue or cross into the blood stream. As evident from several investigations of inhaled TAC in rodents, absorbed TAC molecules seem to preferably remain in lung tissue rather than going into systemic circulation (http://www.fda.gov/ohrms/dockets/ac/05/briefing/2005-4135B1_02_A-FDA-Pulminiq.pdf) (4,18–22,24). The higher lung AUC of TFF TACMAN can be attributed to the faster dissolution rate, leading to more TAC molecules available for absorption into the lung tissue. The overall clearance rate (CL) is much slower for TFF TACMAN compared with micronized TACMAN (data presented in Table I). The nearly 2.3 times greater AUC and slower clearance rate in the lung tissue for TFF TACMAN demonstrated that this formulation is favorable for localized lung delivery, while a micronized formulation may be more susceptible to the lung's clearance mechanisms.

The systemic TAC concentration after exposure to the aerosolized powder of micronized TACMAN and TFF TACMAN is illustrated in Fig. 10. Based on a larger K12 value, the systemic absorption rate of TAC through the lung epithelium is slightly faster for amorphous TFF particles compared to crystalline blend. However, a much higher and more variable blood concentration of TAC was observed for micronized TACMAN compared to TFF TACMAN, likely due to clearance and, subsequently, gastrointestinal (GI) tract absorption. Once deposited, the slowly dissolving micronized crystalline particles undergo mucociliary clearance towards the mouth where they are eventually mixed with saliva and swallowed, then available for absorption via the GI tract into systemic circulation. The more variable blood concentration of TAC that was found for micronized TACMAN at 2 and 4 h was due to its erratic oral bioavailability (varies from 4% to 93%) (61). Additionally, it is possible that the undissolved micronized particles are engulfed by macrophages, which can then be slowly transported along the alveolar surface to the mucociliary escalator or translocation to the interstitium and lymph nodes (35,56). As shown in Fig. 10, besides the first peak concentrations around 1 h, there was a significant second peak at either 4 or 8 h for both experimental groups, which corresponded to the re-absorption of TAC from the GI tract. The calculation of K20 (TAC clearance rate from the blood) is based on the elimination phase in the plasma compartment. However, if TAC was still being absorbed at 8 h, it is not feasible to determine K20 just based on the testing period

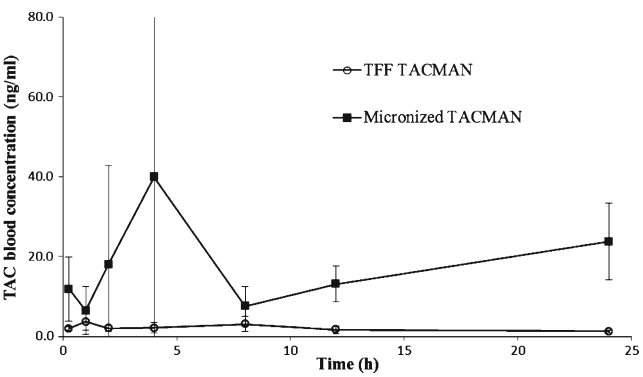


**Fig. 10.** TAC concentration in whole blood following single-dose exposure to dry powder aerosols generated from a rotating brush generator. TFF TACMAN (*open cycle*) and micronized TACMAN (*solid square*)

(up to 24 h) in this study. A slightly increasing trend of TAC concentration in the blood towards the end of the test (from 12 to 24 h) was observed for the micronized group, possibly because the TAC-carrying macrophages slowly moved to the mucociliary escalator and were absorbed orally or TAC transported to the lymphatic system and eventually partitioned into circulation (62). On the other hand, the blood concentration of TAC for TFF TACMAN group remained low (1–5 ng/mL) for the entire testing period (24 h) due to reduced clearance and oral absorption. In summary, by delivering TAC as a more rapidly dissolving formulation, TFF TACMAN is able to provide bioavailable TAC on the pulmonary epithelium and avoid the lung's clearance mechanisms, while minimizing systemic concentration.

## CONCLUSION

Engineered particles containing tacrolimus and mannitol were successfully prepared by TFF. The amorphous TFF-processed formulation demonstrated excellent aerodynamic properties when incorporated into a commercially available DPI. Following a single-dose dry powder inhalation study in a rat model, TFF-processed powders achieved a significantly higher pulmonary bioavailability with longer lung retention time compared to micronized powders, likely due to their ability to avoid pulmonary clearance mechanisms (mucociliary clearance and macrophage uptake). Additionally, lower systemic exposure with small intersubject variability was observed for the TFF-processed formulation, which could potentially reduce adverse side effects. In this study, production of inhaled tacrolimus by TFF has demonstrated the capability to localize therapeutic drug levels to the lungs more effectively than an inhaled micronized blend and minimize systemic level.

## REFERENCES


1. Yusen RD, Christie JD, Edwards LB, Kucheryavaya AY, Benden C, Dipchand AI, *et al*. The registry of the international society for heart and lung transplantation: thirtieth adult lung and heart-lung transplant report-2013; focus theme: age. J Heart Lung Transplant. 2013;32(10):965–78.
2. Boehler A, Estenne M. Obliterative bronchiolitis after lung transplantation. Curr Opin Pulm Med. 2000;6:133–9.
3. Knoop C, Haverich A, Fischer S. Immunosuppressive therapy after human lung transplantation. Eur Respir J. 2004;23(1):159–71.
4. Watts AB, Peters JI, Talbert RL, O'Donnell KP, Coalson JJ, Williams 3rd RO. Preclinical evaluation of tacrolimus colloidal dispersion for inhalation. Eur J Pharm Biopharm. 2011;77(2):207–15.
5. Kino T, Hatanaka H, Miyata S, Inamura N, Nishiyama M, Yajima T, *et al*. FK-506, a novel immunosuppressant isolated from a Streptomyces. II. Immunosuppressive effect of FK-506 in vitro. J Antibiot (Tokyo). 1987;40(9):1256–65.
6. Hariharan S, Peddi VR, Munda R, Demmy AM, Schroeder TJ, Alexander JW, *et al*. Long-term renal and pancreas function with tacrolimus rescue therapy following kidney/pancreas transplantation. Transplant Proc. 1997;29(1–2):652–3.
7. Keenan RJ, Konishi H, Kawai A, Paradis IL, Nunley DR, Iacono AT, *et al.* Clinical trial of tacrolimus versus cyclosporine in lung transplantation. Ann Thorac Surg. 1995;60(3):580–4. discussion 4–5.
8. O'Grady JG, Burroughs A, Hardy P, Elbourne D, Truesdale A, Uk, *et al*. Tacrolimus versus microemulsified ciclosporin in liver transplantation: the TMC randomised controlled trial. Lancet. 2002;360(9340):1119–25.
9. Knoop C, Thiry P, Saint-Marcoux F, Rousseau A, Marquet P, Estenne M. Tacrolimus pharmacokinetics and dose monitoring after lung transplantation for cystic fibrosis and other conditions. Am J Transplant. 2005;5(6):1477–82.
10. Wagner K, Webber SA, Kurland G, Boyle GJ, Miller SA, Cipriani L, *et al*. New-onset diabetes mellitus in pediatric thoracic organ recipients receiving tacrolimus-based immunosuppression. J Heart Lung Transplant. 1997;16(3):275–82.
11. Corcoran TE. Inhaled delivery of aerosolized cyclosporine. Adv Drug Deliv Rev. 2006;58(9–10):1119–27.
12. Groves S, Galazka M, Johnson B, Corcoran T, Verceles A, Britt E, *et al*. Inhaled cyclosporine and pulmonary function in lung transplant recipients. J Aerosol Med Pulm Drug Deliv. 2010;23(1):31–9.
13. Onoue S, Sato H, Kawabata Y, Mizumoto T, Hashimoto N, Yamada S. In vitro and in vivo characterization on amorphous solid dispersion of cyclosporine A for inhalation therapy. J Control Release. 2009;138(1):16–23.
14. Onoue S, Sato H, Ogawa K, Kojo Y, Aoki Y, Kawabata Y, *et al*. Inhalable dry-emulsion formulation of cyclosporine A with improved anti-inflammatory effects in experimental asthma/COPD-model rats. Eur J Pharm Biopharm. 2012;80(1):54–60.
15. Wang T, Noonberg S, Steigerwalt R, Lynch M, Kovelesky RA, Rodriguez CA, *et al*. Preclinical safety evaluation of inhaled cyclosporine in propylene glycol. J Aerosol Med. 2007;20(4):417–28.
16. Behr J, Zimmermann G, Baumgartner R, Leuchte H, Neurohr C, Brand P, *et al*. Lung deposition of a liposomal cyclosporine A inhalation solution in patients after lung transplantation. J Aerosol Med Pulm Drug Deliv. 2009;22(2):121–30.
17. Iacono AT, Johnson BA, Grgurich WF, Youssef JG, Corcoran TE, Seiler DA, *et al*. A randomized trial of inhaled cyclosporine in lung-transplant recipients. N Engl J Med. 2006;354(2):141–50.
18. Ide N, Nagayasu T, Matsumoto K, Tagawa T, Tanaka K, Taguchi T, *et al*. Efficacy and safety of inhaled tacrolimus in rat lung transplantation. J Thorac Cardiovasc Surg. 2007;133(2):548–53.
19. Ingu A, Komatsu K, Ichimiya S, Sato N, Hirayama Y, Morikawa M, *et al*. Effects of inhaled FK 506 on the suppression of acute rejection after lung transplantation: use of a rat orthotopic lung transplantation model. J Heart Lung Transplant. 2005;24(5):538–43.
20. Morishita Y, Hirayama Y, Miyayasu K, Tabata K, Kawamura A, Ohkubo Y, *et al*. FK506 aerosol locally inhibits antigen-induced airway inflammation in guinea pigs. Int Arch Allergy Immunol. 2005;136(4):372–8.
21. Deuse T, Blankenberg F, Haddad M, Reichenspurner H, Phillips N, Robbins RC, *et al*. Mechanisms behind local immunosuppression using inhaled tacrolimus in preclinical models of lung transplantation. Am J Respir Cell Mol Biol. 2010;43(4):403–12.
22. Schrepfer S, Deuse T, Reichenspurner H, Hoffmann J, Haddad M, Fink J, *et al*. Effect of inhaled tacrolimus on cellular and humoral rejection to prevent posttransplant obliterative airway disease. Am J Transplant. 2007;7(7):1733–42.
23. Sinswat P, Overhoff KA, McConville JT, Johnston KP, Williams 3rd RO. Nebulization of nanoparticulate amorphous or crystalline tacrolimus–single-dose pharmacokinetics study in mice. Eur J Pharm Biopharm. 2008;69(3):1057–66.
24. Watts AB, Cline AM, Saad AR, Johnson SB, Peters JI, Williams 3rd RO. Characterization and pharmacokinetic analysis of tacrolimus dispersion for nebulization in a lung transplanted rodent model. Int J Pharm. 2010;384(1–2):46–52.
25. Chougule M, Padhi B, Misra A. Nano-liposomal dry powder inhaler of tacrolimus: preparation, characterization, and pulmonary pharmacokinetics. Int J Nanomedicine. 2007;2(4):675–88.
26. Watts AB, Wang YB, Johnston KP, Williams 3rd RO. Respirable low-density microparticles formed in situ from aerosolized brittle matrices. Pharm Res. 2013;30(3):813–25.
27. Edwards DA, Hanes J, Caponetti G, Hrkach J, Ben-Jebria A, Eskew ML, *et al*. Large porous particles for pulmonary drug delivery. Science. 1997;276(5320):1868–71.
28. Vanbever R, Mintzes JD, Wang J, Nice J, Chen D, Batycky R, *et al*. Formulation and physical characterization of large porous particles for inhalation. Pharm Res. 1999;16(11):1735–42.
29. Dellamary LA, Tarara TE, Smith DJ, Woelk CH, Adractas A, Costello ML, *et al*. Hollow porous particles in metered dose inhalers. Pharm Res. 2000;17(2):168–74.

30. Duddu SP, Sisk SA, Walter YH, Tarara TE, Trimble KR, Clark AR, *et al*. Improved lung delivery from a passive dry powder inhaler using an engineered PulmoSphere powder. Pharm Res. 2002;19(5):689–95.
31. Richardson PC, Boss AH. Technosphere insulin technology. Diabetes Technol Ther. 2007;9 Suppl 1:S65–72.
32. Plumley C, Gorman EM, El-Gendy N, Bybee CR, Munson EJ, Berkland C. Nifedipine nanoparticle agglomeration as a dry powder aerosol formulation strategy. Int J Pharm. 2009;369(1–2):136–43.
33. Geiser M. Update on macrophage clearance of inhaled micro- and nanoparticles. J Aerosol Med Pulm Drug Deliv. 2010;23(4):207–17.
34. Yang W, Johnston KP, Williams 3rd RO. Comparison of bioavailability of amorphous versus crystalline itraconazole nanoparticles via pulmonary administration in rats. Eur J Pharm Biopharm. 2010;75(1):33–41.
35. Olsson B, Bondesson E, Borgstrom L. Pulmonary drug metabolism, clearance, and absorption. In: Controlled pulmonary drug delivery [Internet]. New York, NY: Springer; 2011. 1. Available from: doi:10.1007/978-1-4419-9745-6.
36. Mobley C, Hochhaus G. Methods used to assess pulmonary deposition and absorption of drugs. Drug Discov Today. 2001;6(7):367–75.
37. Esmailpour N, Hogger P, Rabe KF, Heitmann U, Nakashima M, Rohdewald P. Distribution of inhaled fluticasone propionate between human lung tissue and serum in vivo. Eur Respir J. 1997;10(7):1496–9.
38. Thorsson L, Edsbacker S, Kallen A, Lofdahl CG. Pharmacokinetics and systemic activity of fluticasone via Diskus and pMDI, and of budesonide via Turbuhaler. Br J Clin Pharmacol. 2001;52(5):529–38.
39. Engstrom JD, Lai ES, Ludher BS, Chen B, Milner TE, Williams 3rd RO, *et al*. Formation of stable submicron protein particles by thin film freezing. Pharm Res. 2008;25(6):1334–46.
40. Ball DJ, Hirst PH, Newman SP, Sonet B, Streel B, Vanderbist F. Deposition and pharmacokinetics of budesonide from the Miat Monodose inhaler, a simple dry powder device. Int J Pharm. 2002;245(1–2):123–32.
41. Mitchell JP. Practices of coating collection surfaces of cascade impactors: a survey of members of the European Pharmaceutical Aerosol Group (EPAG). Drug Deliv Lung. 2003;14:75–8.
42. Marple VA, Olson BA, Santhanakrishnan K, Mitchell JP, Murray SC, Hudson-Curtis BL. Next generation pharmaceutical impactor (a new impactor for pharmaceutical inhaler testing). Part II: Archival calibration. J Aerosol Med. 2003;16(3):301–24.
43. Moyano MA, Simionato LD, Pizzorno MT, Segall AI. Validation of a liquid chromatographic method for determination of tacrolimus in pharmaceutical dosage forms. J AOAC Int. 2006;89(6):1547–51.
44. USP 32-NF 27 General Chapter 601: Aerosols, nasal sprays, metered-dose inhalers, and dry powder inhalers. 218–39.
45. Gombás A, Szabó-Révész P, Kata M, RJ G, Erõs I. Quantitative determination of crystallinity of a-lactose monohydrate by DSC. J Therm Anal Calorim. 2002;68:503–10.
46. Hilden LR, Morris KR. Physics of amorphous solids. J Pharm Sci. 2004;93(1):3–12.
47. Deng Z, Xu S, Li S. Understanding a relaxation behavior in a nanoparticle suspension for drug delivery applications. Int J Pharm. 2008;351(1–2):236–43.
48. Kim AI, Akers MJ, Nail SL. The physical state of mannitol after freeze-drying: effects of mannitol concentration, freezing rate, and a noncrystallizing cosolute. J Pharm Sci. 1998;87(8):931–5.
49. Zidan AS, Rahman Z, Sayeed V, Raw A, Yu L, Khan MA. Crystallinity evaluation of tacrolimus solid dispersions by chemometric analysis. Int J Pharm. 2012;423(2):341–50.
50. Zhao M, Barker SA, Belton PS, McGregor C, Craig DQ. Development of fully amorphous dispersions of a low T(g) drug via co-spray drying with hydrophilic polymers. Eur J Pharm Biopharm. 2012;82(3):572–9.
51. Rasenack N, Muller BW. Micron-size drug particles: common and novel micronization techniques. Pharm Dev Technol. 2004;9(1):1–13.
52. Saleem IY, Smyth HD. Micronization of a soft material: air-jet and micro-ball milling. AAPS PharmSciTech. 2010;11(4):1642–9.
53. Rogueda PG, Traini D. The nanoscale in pulmonary delivery. Part 1: deposition, fate, toxicology and effects. Expert Opin Drug Deliv. 2007;4(6):595–606.
54. de Villiers MM. Influence of cohesive properties of micronized drug powders on particle size analysis. J Pharm Biomed Anal. 1995;13(3):191–8.
55. Byron PR. Prediction of drug residence times in regions of the human respiratory tract following aerosol inhalation. J Pharm Sci. 1986;75(5):433–8.
56. Zhang J, Wu L, Chan HK, Watanabe W. Formation, characterization, and fate of inhaled drug nanoparticles. Adv Drug Deliv Rev. 2011;63(6):441–55.
57. Alexander DJ, Collins CJ, Coombs DW, Gilkison IS, Hardy CJ, Healey G, *et al*. Association of Inhalation Toxicologists (AIT) working party recommendation for standard delivered dose calculation and expression in non-clinical aerosol inhalation toxicology studies with pharmaceuticals. Inhal Toxicol. 2008;20(13):1179–89.
58. Kuehl PJ, Anderson TL, Candelaria G, Gershman B, Harlin K, Hesterman JY, *et al*. Regional particle size dependent deposition of inhaled aerosols in rats and mice. Inhal Toxicol. 2012;24(1):27–35.
59. Edwards DA, Ben-Jebria A, Langer R. Recent advances in pulmonary drug delivery using large, porous inhaled particles. J Appl Physiol. 1998;85(2):379–85.
60. Lehnert BE, Morrow PE. Association of 59iron oxide with alveolar macrophages during alveolar clearance. Exp Lung Res. 1985;9(1–2):1–16.
61. Venkataramanan R, Shaw LM, Sarkozi L, Mullins R, Pirsch J, MacFarlane G, *et al*. Clinical utility of monitoring tacrolimus blood concentrations in liver transplant patients. J Clin Pharmacol. 2001;41(5):542–51.
62. Shin SB, Cho HY, Kim DD, Choi HG, Lee YB. Preparation and evaluation of tacrolimus-loaded nanoparticles for lymphatic delivery. Eur J Pharm Biopharm. 2010;74(2):164–71.